AIR–SEA FLUX ESTIMATES AND THE 1997–1998 ENSO EVENT**

A. BIROL KARA
Center for Ocean-Atmospheric Prediction Studies, The Florida State University, Tallahassee, Florida 32306, U.S.A.

PETER A. ROCHFORD* and HARLEY E. HURLBURT
Oceanography Division, Naval Research Laboratory, Stennis Space Center, Mississippi 39529, U.S.A.

(Received in final form 31 August 2001)

Abstract. Bulk formulae for wind stress, sensible and latent heat flux are presented that are suitable for strong mesoscale events such as westerly wind bursts that contribute to the El Niño-Southern Oscillation (ENSO). Their exchange coefficients for heat and momentum have a simple polynomial dependence on wind speed and a linear dependence on air–sea temperature difference. The accuracy of these formulae are validated with respect to air–sea fluxes estimated using the standard algorithm adopted by the Tropical Ocean-Global Atmosphere Coupled-Ocean Atmosphere Response Experiment (TOGA COARE). The comparison is made for observations from 96 Tropical Atmosphere Ocean (TAO) array and National Oceanographic Data Center (NODC) moorings in the equatorial and North Pacific Ocean spanning years 1990–1999. The bulk formulae are shown to have very small median root–mean-square differences with respect to the TOGA COARE estimates: ≈ 0.003 N m^{-2}, 1.0 W m^{-2}, and 10.0 W m^{-2} for the wind stress, sensible heat flux, and latent heat flux, respectively.

The variability of air–sea fluxes during the 1997–1998 ENSO is also examined, along with a possible relationship between air–sea fluxes and surface ocean mixed layer depth (MLD). The wind stress and latent heat flux during the 1997 El Niño are found to be greater in the warm pool of the western Pacific than in the central Pacific where the ENSO is most clearly seen. These differences disappear upon the start of La Niña. The MLD in the equatorial Pacific is found to be moderately correlated to air–sea fluxes just before the start of the 1998 La Niña and poorly correlated otherwise.

Keywords: Bulk formulae, El Niño, La Niña, Latent and sensible heat flux, Ocean mixed-layer depth, Wind stress.

1. Introduction

Previously, efficient and computationally inexpensive bulk formulae were presented for wind stress, sensible and latent heat flux (Kara et al., 2000a), and were shown to be comparable in accuracy with those obtained using the standard algorithm adopted for the Tropical Ocean-Global Atmosphere Coupled-Ocean Atmosphere Response Experiment (TOGA COARE) as described in Fairall et al. (1996). This comparison was performed using 1994-1995 meteorological obser-

* Corresponding author. E-mail: rochford@nrlssc.navy.mil

Boundary-Layer Meteorology **103:** 439–458, 2002.

vations from a moored buoy in the Arabian Sea (Weller et al., 1998) for which shortwave and longwave radiative fluxes at the air–sea surface were available. The availability of the radiative fluxes allowed cool skin and warm layer effects to be taken into account. Unfortunately, the temperature corrections for the latter cannot be included when determining air–sea fluxes* for the vast majority of buoys deployed operationally for weather forecasting, because information on the radiative fluxes is rarely available (McPhaden, 1995). While air–sea fluxes can still be determined using the TOGA COARE algorithm without these corrections, the need for simultaneous observations of several quantities (wind speed, air humidity, air temperature, water temperature, and air pressure) often results in no air–sea flux estimates for large time periods in the mooring record. This is because one or more of the required quantities is frequently unavailable due to sensor failure. For this reason we present here revised versions of our bulk formulae for air–sea fluxes that are adjusted to more closely reproduce the TOGA COARE estimates in the absence of cool skin and warm layer effects.

We test the new bulk formulae by comparing them against the TOGA COARE fluxes during the strong mesoscale events of an El Niño and La Niña. The El Niño–Southern Oscillation (ENSO) is a manifestation of a strong physical coupling between the tropical atmosphere and the waters of the Pacific Ocean. During this coupled interaction the wind stress and heat fluxes at the air–sea interface play an important role because they provide heat and momentum exchange between the atmosphere and ocean (e.g., Sun, 2000). Since this exchange process is highly variable during an ENSO, event an accurate parameterization of the air–sea fluxes that is computationally efficient would be of value for numerically intensive coupled atmosphere–ocean general circulation models (GCMs) that seek to describe ENSO phenomena. We specifically use buoy observations in the equatorial Pacific when testing our formulae because the greatest strength and impact of the ENSO occurs in this region (McPhaden, 1999; Meinen and McPhaden, 2000).

Given that air–sea fluxes are primarily responsible for the turbulent mixing that produces the surface mixed layer, we also investigate a possible relationship between these air–sea fluxes and surface ocean mixed-layer depth (MLD). This is relevant because studies using numerical models have identified changes in the thermocline or surface mixed layer as often playing an important role in the ENSO mediated physical processes (Yukimoto et al., 1996; Perigaud et al., 2000; Cassou and Perigaud, 2000). For example, thermocline depth anomalies have been shown to be important for simulating and identifying the eastward propagation of El Niño warm events in the upper ocean (White and McCreary, 1974; Hurlburt et al. 1976; Zhang and Busalacchi, 1999; White and Cayan, 2000). Seeking such a relationship is further motivated by air–sea turbulent heat exchange being an important mechanism for sea surface temperature (SST) anomalies during ENSO (Weisberg and Wang, 1997). Wind stress is of particular importance because it is the leading

* Hereinafter we will refer to the wind stress, sensible and latent heat fluxes as air–sea fluxes.

contributor to turbulent kinetic energy generated in the mixed layer and because the amount of heat stored in the ocean is most sensitive to its contribution (O'Brien and Horsfall, 1995).

In Section 2 we present our revised parameterizations for the air–sea fluxes. In Section 3 we validate the formulae by directly comparing our estimated air–sea fluxes with respect to those obtained using the TOGA COARE algorithm for a large number of widely distributed buoys in the equatorial and North Pacific. Section 4 gives an overview of the 1997–1998 ENSO and examines the performance of our formulae during this event. We then use the latter and subsurface mooring observations in Section 5 to explore the relationship between air–sea fluxes and MLD during the 1997–1998 ENSO event. Finally, we present our conclusions in Section 6.

2. Air–Sea Flux Parameterization

To determine the air–sea fluxes we use exchange coefficients for heat and momentum (i.e., C_D, C_L, and C_S) that have a simple polynomial dependence on wind speed, and a linear dependence on the air–sea temperature difference. A quadratic or higher order dependence on wind speed is necessary because a drag coefficient with a linear dependence on wind speed has been shown to be inadequate (Blake, 1991). We determine these new coefficients using the same methodology as in Kara et al. (2000a) with the exception of using modified exchange coefficient values from Isemer et al. (1989) that are approximately 18% less than those provided by Bunker (1976). This adjustment was made to accurately parameterize these fluxes in the absence of skin temperature effects. We elect to use this approach rather than more advanced methods such as the standard algorithm used by the TOGA COARE because the individual exchange coefficients depend upon fewer variables, are 27–29 times faster to calculate, and provide sufficient accuracy for most scientific applications (Kara et al., 2000a). The formulae we present below can also be used to supplement the TOGA COARE fluxes on the many occasions when there is insufficient meteorology for the algorithm to provide an estimate. For a discussion of exchange coefficients used in traditional bulk flux parameterizations the reader is referred to Smith (1989) and Smith et al. (1996).

The wind stress (τ) is calculated via the relations

$$\tau = \rho_a C_D (u^2 + v^2), \tag{1}$$

$$C_D = C_{D0} + C_{D1}(T_s - T_a), \tag{2}$$

$$C_{D0} = 10^{-3}\left[0.692 + 0.071\widehat{V}_a - 0.00070(\widehat{V}_a)^2\right], \tag{3}$$

$$C_{D1} = 10^{-3}\left[0.083 - 0.0054\widehat{V}_a + 0.000093(\widehat{V}_a)^2\right], \tag{4}$$

while the latent heat flux (Q_L) and sensible heat flux (Q_S) are computed via the equations

$$Q_S = C_S C_p \rho_a V_a (T_a - T_s), \tag{5}$$

$$Q_L = C_L L \rho_a V_a (q_a - q_s), \tag{6}$$

$$C_L = C_{L0} + C_{L1}(T_s - T_a), \tag{7}$$

$$C_{L0} = 10^{-3}\left[0.8195 + 0.0506\widehat{V}_a - 0.0009(\widehat{V}_a)^2\right], \tag{8}$$

$$C_{L1} = 10^{-3}\left[-0.0154 + 0.5698(1/\widehat{V}_a) - 0.6743(1/\widehat{V}_a)^2\right]. \tag{9}$$

V_a is wind speed at 10 m above sea level; zonal and meridional wind speed components are denoted as u and v, respectively; C_p is specific heat of air (1004.5 J kg^{-1} K^{-1}); and L is latent heat of vaporization (2.5×10^6 J kg^{-1}).

Limits are set on the wind speed as $\widehat{V}_a = \max[2.5, \min(32.5, V_a)]$ because the drag coefficient is constant when $V_a > 35$ m s^{-1}. We also used this limit to overcome the break down of the bulk aerodynamic formulae when winds are calm (Godfrey and Beljaars, 1991). These equations have been derived for a wind speed measured at a reference height of 10 m above the sea surface. We previously found $C_S = 0.95C_L$ to work very well and use this exchange coefficient here accordingly. This ratio is also consistent with the one suggested in a previous study (Dunckel et al., 1974). The air density (in kg m^{-3}) is determined using the ideal gas law: $\rho_a = 100P_a/[R_{\text{gas}}(T_a + 273.16)]$, where P_a is set to 1013 hPa. While in principle the potential temperature should be used to calculate sensible heat flux (see Equation (5)), the difference is usually insignificant at the 10-m height. In estimating the sensible and latent heat flux we define SST to be the temperature at 1-m depth. While it is preferable to use the adjusted ocean skin temperature for the SST, we assume that using a 1-m depth temperature for SST will yield reasonable estimates in our bulk scheme based on Lee et al. (1998).

As mentioned previously, the calculation of air–sea fluxes with these bulk formulae have been shown to be 27–29 times faster than using the TOGA COARE algorithm. The greater amount of cpu time required by that algorithm is proportional to the 20 iterations required by the latter for its atmospheric surface-layer calculations of roughness and stability. Computational efficiency makes the bulk formulae used here a preferred choice for use in any numerically intensive ocean or atmosphere GCM of high spatial resolution.

Finally, we note that a bulk formula has been derived for wind stress as a function of both wind speed and significant wave height (H) by Blake (1991). The dependence of the latter on wind speed for the H-independent portion of the drag coefficient is similar to our C_{D0} (Equation (3)), but has numerical values that are larger by 1.36 to 5.7 times. Including wave height dependence yields only marginally better results than those obtained using a bulk formula based solely on

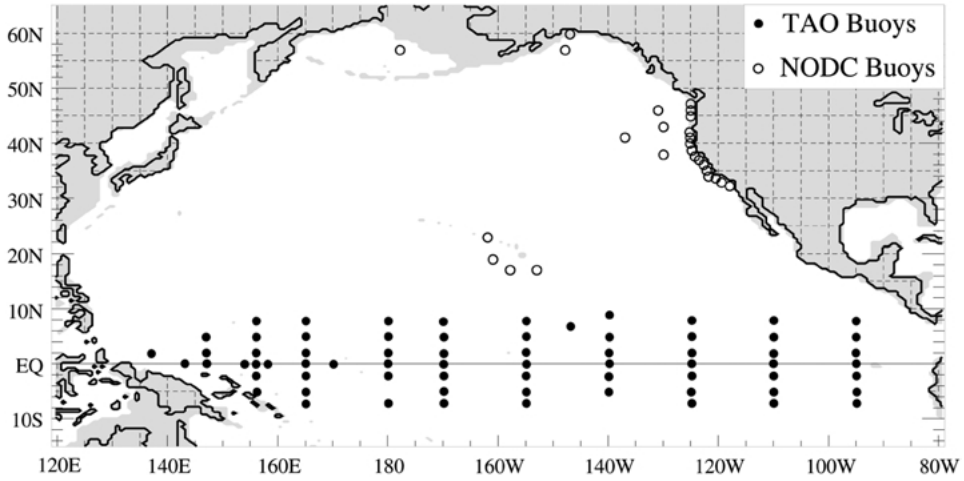

Figure 1. TAO array and NODC buoys used for verification of air–sea fluxes. The TAO buoys (63 of them) provide the larger sampling and are located in the equatorial Pacific Ocean. The NODC buoys (33 of them) provide sampling outside the equatorial Ocean and are located off the coasts of the continental U.S., Hawaii and Alaska.

wind speed (Blake, 1991). The latter result might be because an air–sea temperature dependence was not included.

3. Air–Sea Flux Validation

To validate our bulk formulae we use meteorological observables provided by the Tropical Atmosphere Ocean (TAO) array (McPhaden, 1995) and National Oceanographic Data Center (NODC) moorings for the years 1990–1999 (Figure 1). TAO and NODC have deployed a total of 96 buoys throughout the equatorial and North Pacific Ocean and we use all available meteorological data for our validation. The wide distribution of the buoys and their lengthy mooring records provide an ample source of data from which to test our formulae in both open ocean (TAO buoys) and coastal regions (NODC buoys) during long time periods. Each buoy provides a time series of surface air and sea temperatures, air specific humidity and wind velocity, with the time period sampled in each mooring record varying according to buoy deployment period and functioning sensor operation. Air–sea fluxes are not computed for periods where any single meteorological observable required by the TOGA COARE algorithm is missing, and no averaging or smoothing is applied to the original observables prior to determining the air–sea fluxes.

For the validation procedure we construct air–sea fluxes from the buoy meteorology using our bulk formulae (Equations (1)–(9)) and the TOGA COARE algorithm. The latter is used to obtain reference (observed) air–sea fluxes because it is a state-of-the-art algorithm for estimating the wind stress, sensible and latent heat

fluxes. The algorithm employs a turbulence theory based on the classical Monin–Obukhov similarity approach, along with detailed parameterizations, to determine stability-dependent exchange coefficients of heat and momentum (Fairall et al., 1996). The algorithm also provides meteorology adjusted to a standard reference height that is usually set at 10 m. The availability of the TOGA COARE algorithm along with the TAO and NODC meteorology makes this an ideal approach by which to verify our formulae and assess their accuracy relative to a fully stability-dependent formulation. We compute air–sea fluxes using both methods for the 1990–1999 mooring record of each TAO and NODC buoy and then (to reduce data volume) construct daily averages for the comparisons.

The mixing ratio values for air (q_a at T_a) and sea (q_s at T_s) are calculated using a simplified version of the original formulation for saturated vapour pressure (e_s) presented by Buck (1981). Similar to the air and sea mixing ratio, e_s is also calculated at T_a and T_s for air and sea, respectively. Note that for consistency we adjust all meteorology to a 10-m reference height using the TOGA COARE algorithm before substitution into our aerodynamic bulk formulae. The ocean temperature at 1-m depth is used for the sea surface temperature and this is provided by the buoy data. While it would be better to estimate latent heat flux using the ocean skin temperature because of the cool skin and warm layer effects as explained in Fairall et al. (1996), Zeng et al. (1998) have shown that a bulk formula that excludes such effects can produce comparable results. They found the differences between inclusion and exclusion of these corrections to be only a few W m^{-2}.

To measure the strength of the relationship between the air–sea fluxes predicted by our method and those from the standard TOGA COARE algorithm we use various statistical metrics. For what follows let X_i ($i = 1, 2, \ldots, N$) be the set of N air–sea flux values calculated from the TOGA COARE algorithm, and let Y_i ($i = 1, 2, \ldots, N$) be the set of corresponding estimates from our formulae. Also let $\overline{X}(\overline{Y})$ and $\sigma_X(\sigma_Y)$ be the mean and standard deviations of the reference (estimate) values, respectively. Here N is the number of daily averaged air–sea fluxes in the mooring time series for each buoy and year according to data availability. Given these definitions, we can express the statistical relationships between TOGA COARE and our estimates as follows (e.g., Murphy, 1988):

$$\mathrm{ME} = \overline{Y} - \overline{X}, \tag{10}$$

$$\mathrm{RMS} = \left[\frac{1}{N}\sum_{i=1}^{N}(Y_i - X_i)^2\right]^{1/2}, \tag{11}$$

$$R = \frac{1}{N}\sum_{i=1}^{N}(X_i - \overline{X})(Y_i - \overline{Y})/(\sigma_X\sigma_Y), \tag{12}$$

$$\mathrm{SS} = R^2 - \underbrace{[R - (\sigma_Y/\sigma_X)]^2}_{B_{\mathrm{cond.}}} - \underbrace{[(\overline{Y} - \overline{X})/\sigma_X]^2}_{B_{\mathrm{uncond.}}}, \tag{13}$$

TABLE I

Error statistics between wind stress values obtained from the bulk formulae and the TOGA COARE algorithm.

Wind stress τ	ME (N m^{-2})	RMS (N m^{-2})	R	SS
(0°Eq, 110°W)	−0.001	0.001	0.99	0.99
(0°Eq, 165°E)	−0.002	0.002	0.99	0.99
(02°N, 155°W)	−0.002	0.002	0.99	0.99
(05°N, 170°W)	−0.001	0.002	0.99	0.99
(08°S, 125°W)	−0.001	0.002	0.99	0.99
(08°S, 165°E)	−0.001	0.002	0.99	0.99
(34°N, 120°W)	0.004	0.005	0.99	0.99
(35°N, 121°*W*)	0.001	0.003	0.99	0.99

where, ME is the mean error, RMS is the root-mean-square difference, R is the correlation coefficient, and SS is the skill score. Note here that SS involves bias (conditional bias, $B_{\text{cond.}}$, and unconditional bias, $B_{\text{uncond.}}$) that is not taken into account in the correlation coefficient. Because these two bias terms are never negative, the correlation coefficient can be considered to be a measure of 'potential' skill, i.e., the skill we can obtain by eliminating bias from our method. SS = 1 for perfect estimates and is negative if our estimates are poor relative to those obtained using TOGA COARE.

The error statistics for several TAO and NODC buoys are shown in Tables I and II to illustrate how well our bulk formulae reproduce the TOGA COARE air–sea fluxes over different regions of the north Pacific Ocean. In addition to very small ME and RMS overall, our method is able to capture well the phase of the daily air–sea flux variability ($R \approx 1$ in most cases). Very large SS values that are close to 1 indicate that the formulae are able to produce air–sea fluxes with an acceptable accuracy for all locations.

Applying the same statistical analysis as presented in Tables I and II, we generate median statistics for all available buoys to assess the general performance of our formulae with respect to the TOGA COARE algorithm. The statistical analysis is performed for the 63 NODC and 33 TAO buoys as separate groups. To obtain modal (median) statistics we then combine the individual ME, RMS, R and SS values from all buoys under one category to calculate cumulative frequency. As an example, Figure 2 shows the latent heat flux distribution for all TAO buoys. The median ME and RMS difference for Q_L at the TAO buoys is only 1.3 W m^{-2} and 10.9 W m^{-2}, respectively. The median SS value of 0.91 demonstrates how well the formula performs overall in reproducing the variability in the time series with

TABLE II

Error statistics between sensible heat flux and latent heat flux values obtained from the bulk formulae and the TOGA COARE algorithm.

Sensible heat Q_S	ME (W m^{-2})	RMS (W m^{-2})	R	SS
(0°Eq, 110°W)	0.3	0.6	0.99	0.98
(0°Eq, 165°E)	−0.2	1.4	0.98	0.97
(02°N, 155°W)	0.2	0.8	0.98	0.97
(05°N, 170°W)	0.2	1.1	0.99	0.97
(08°S, 125°W)	0.7	0.9	0.99	0.93
(08°S, 165°E)	0.2	1.0	0.99	0.97
(34°N, 120°W)	1.5	2.7	0.99	0.92
(35°N, 121°W)	0.3	1.3	0.98	0.97
Latent heat Q_L	ME (W m^{-2})	RMS (W m^{-2})	R	SS
(0°Eq, 110°W)	1.7	5.9	0.99	0.98
(0°Eq, 165°E)	−4.2	14.7	0.98	0.89
(02°N, 155°W)	0.2	10.7	0.98	0.93
(05°N, 170°W)	2.2	12.6	0.97	0.89
(08°S, 125°W)	6.5	12.9	0.97	0.88
(08°S, 165°E)	1.9	13.3	0.97	0.91
(34°N, 120°W)	10.7	15.7	0.98	0.78
(35°N, 121°W)	4.4	8.1	0.98	0.84

a small bias. The overall error statistics (Table III) for τ, Q_L and Q_S have small median values for the ME and RMS differences. Median values of R greater than 0.98 and median values of SS ≈ 1 validate further the accuracy of our formulae.

4. Air–Sea Fluxes during 1997–1998 ENSO Event

We first describe the 1997–1998 ENSO event to define the time periods for the El Niño and La Niña. ENSO extremes usually develop in boreal winter or early summer and persist through the following winter. Although there is no universally accepted definition of El Niño (i.e., warm SST anomalies in the Pacific) and La Niña (i.e., cold SST anomalies), one commonly used definition is the Japan Meteorological Agency (JMA) index, which is calculated with respect to SST in the eastern Pacific (Smith et al., 1999). SSTs in the eastern equatorial Pacific Ocean

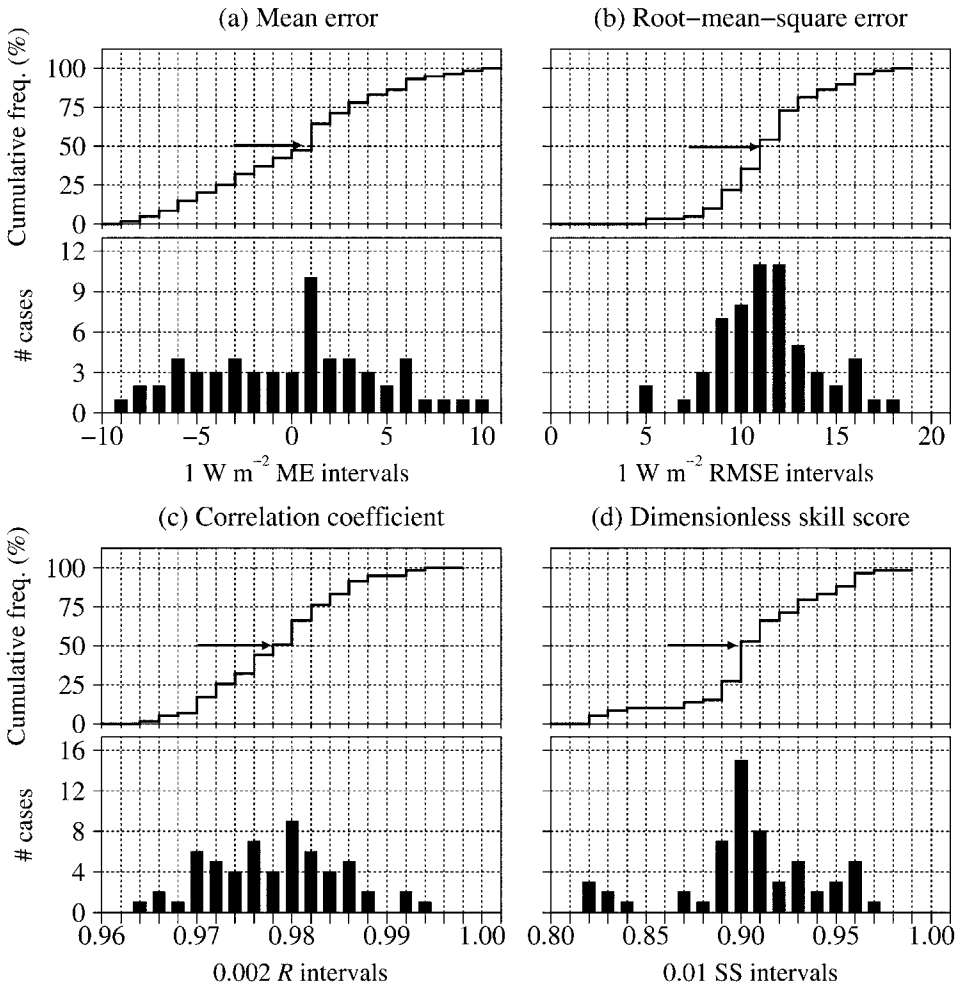

Figure 2. Cumulative frequency and total number of cases between latent heat fluxes obtained from the formulae presented in this paper relative to the TOGA COARE algorithm: (a) Mean error (ME) in °C, (b) root-mean-square (RMS) difference in °C, (c) correlation coefficient (R), and (d) nondimensional skill score (SS). The horizontal arrow indicates the median value.

are a more reliable indicator of ENSO phase than the Southern Oscillation Index (SOI), which is defined as the sea level pressure anomaly difference between Tahiti and Darwin. The JMA index based on spatially-averaged SST anomalies over the tropical Pacific Ocean selects ENSO events with greater fidelity (Elsner and Kara, 1999; Wang and Weisberg, 2000). The SOI varies considerably from month to month, and large month-to-month variations in the SOI make detecting the phase of ENSO difficult with this index alone. Thus, SSTs in the eastern equatorial Pacific Ocean are usually preferred, and are used here to calculate the JMA index over the period 1949 through 1998.

TABLE III

Median error statistics between wind stress, sensible heat and latent heat flux values obtained from the bulk formulae and the TOGA COARE algorithm. Values in parentheses are standard deviations. Median values are obtained for the 63 TAO and 33 NODC buoys.

Wind stress τ	ME (N m^{-2})	RMS (N m^{-2})	R	SS
TAO	−0.001	0.002	0.99	0.99
	(0.001)	(0.031)	(0.001)	(0.001)
NODC	0.002	0.004	0.99	0.99
	(0.003)	(0.144)	(0.005)	(0.012)
Wind stress Q_S	ME (N m^{-2})	RMS (N m^{-2})	R	SS
TAO	0.17	0.97	0.99	0.97
	(0.35)	(0.20)	(0.01)	(0.02)
NODC	0.62	1.75	0.99	0.97
	(0.59)	(0.75)	(0.01)	(0.02)
Latent heat Q_L	ME (N m^{-2})	RMS (N m^{-2})	R	SS
TAO	1.31	10.96	0.98	0.91
	(4.55)	(2.71)	(0.01)	(0.04)
NOD	5.92	11.51	0.98	0.88
	(3.08)	(3.38)	(0.01	(0.05)

The JMA index is a 5-month running mean of spatially averaged SST anomalies over the tropical Pacific from 4°S–4°N and 150°W–90°W. If the index values are 0.5 °C or greater for six consecutive months that include October, November, and December, then the ENSO year of October through the following September is categorized as having an El Niño event. JMA index values that are less than −0.5 °C indicate a cold ENSO phase. Figure 3 shows SST anomalies calculated using the JMA index for each month during 1996–1998 and clearly reveals the 1997–1998 El Niño lasting 13 months from May 1997 through May 1998. By late summer of 1998 this El Niño had been replaced by La Niña. The neutral ENSO phase (SST anomalies are between −0.5 and 0.5 °C) is evident during June, July, and August 1998. We note that the 1997–1998 ENSO event was approximately of the same strength as the very strong 1982–1983 El Niño, but developed much more rapidly with a record high SST anomaly occurring in the equatorial Pacific.

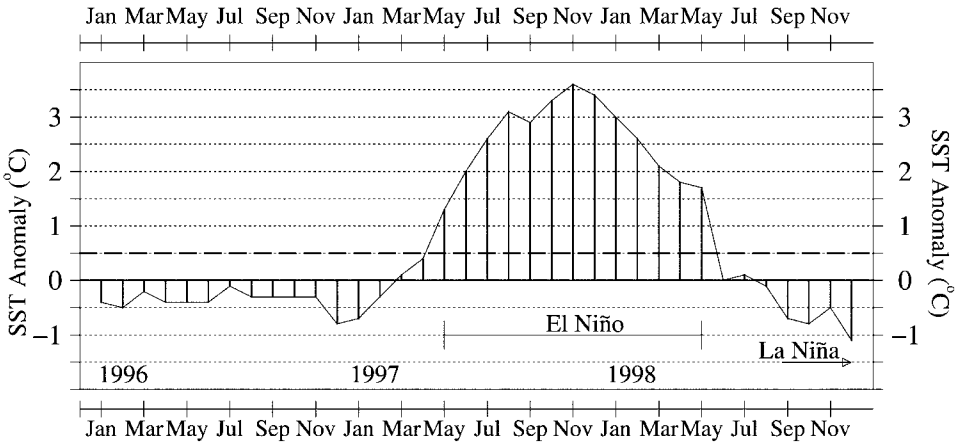

Figure 3. SST anomalies by month for the period January 1996 through January 1999. The anomalies have been calculated using the Japan Meteorological Agency (JMA) index. The duration of the 1997 El Niño and 1998 La Niña events are indicated using the JMA index criteria. Values above the dashed line are the anomalies greater than 0.5 °C. JMA index values that are less than – 0.5 °C indicate a cold phase. The interested reader is referred to Elsner and Kara (1999) for phases of historical ENSO based on values of the JMA index.

We determine the air–sea fluxes using our bulk formulae and the meteorology from several TAO moorings (McPhaden, 1995). The required surface data from the TAO buoys includes air temperature (T_a), SST (T_s), wind speed (V_a), wind direction (ϕ), and relative humidity (RH). Daily averages of these physical quantities are calculated from the observational records that are at 10-min sampling intervals. The air temperature and wind speed are measured at a height of 3.8 m above the sea surface. Rainfall (P) is obtained with RM Young capacitance rain gauges at 1-minute intervals, which we average to daily values. When the wind speed is about 10 m s^{-1} the rainfall is subject to a wind speed bias that is approximately ±20%. Shortwave radiation is measured at a relative accuracy of 3% using an Eppley pyranometer that samples at 1-second intervals, and averages at 2-min intervals, from 0600–1800 local time each day. The daily mean is computed from measurements made between 0000 and 2359 GMT of the indicated day. In this study we use the 2-min averaged solar radiation for the daily means.

Figure 4 shows the time series of the buoy data at (5°N, 165°E) from July 1997 through November 1998. This mooring is chosen because it is located in the warm pool of the western Pacific and allows us to test the accuracy of our relations when the effects of rainfall are included. July 1997 is chosen (i.e., two months after the El Niño started) because no rainfall data are available prior to this time. The relative humidity is largest during the early stages of La Niña and does not show much variability. Note that rainfall was relatively large just after the beginning of the El Niño and La Niña. For computing the air–sea fluxes with our bulk formulae the required buoy observables are wind speed, temperature, and

mixing ratio differences between air and sea. The q_a and q_s values are calculated using RH through T_a, T_s, and the surface atmospheric pressure. Because rainfall can transfer appreciable wind stress to the ocean surface (Gosnell et al., 1995), we checked whether it had a significant contribution by computing $\tau_r = RV_a/3600$, where R is the rain rate in millimetres per hour and the water density is implicit (Caldwell and Elliott, 1971). We found this contribution to be negligible.

The air–sea fluxes for the buoys at (5°N, 165°E) and (0°Eq, 170°W) are shown in Figure 5. We include the central Pacific buoy at (0°Eq, 170°W) to compare the response in the warm pool against the response at a location where the ENSO is clearly seen. Both τ and Q_L are greater overall at (5°N, 165°E) than at (0°Eq, 170°W) during the 1997 El Niño. However, as soon as La Niña starts these significant differences disappear between like quantities at the two locations. To determine the accuracy of our air–sea fluxes at these two buoys we compare τ, Q_L and Q_S computed with Equations (1), (5) and (6) against those obtained from the TOGA COARE algorithm when using contemporaneous data from the same buoys. The standard algorithm includes the effect of dynamic stability in calculating the wind stress and air–sea heat fluxes. A scatter plot (Figure 6) clearly shows good agreement between our estimate and the TOGA COARE reference values for the two TAO buoys. At (5°N, 165°E) the RMS differences are 0.002 N m^{-2}, 12.8 W m^{-2}, and 1.0 W m^{-2} for τ, Q_L, and Q_S, respectively. Similarly, at (0°Eq, 170°W) there are small RMS differences of 0.002 N m^{-2}, 11.7 W m^{-2}, and 0.9 W m^{-2} for τ, Q_L, and Q_S respectively.

5. Air–Sea Flux and Ocean MLD Relationship

Ocean mixed-layer depth (MLD) is primarily determined by turbulent mixing due to forcing at the air–sea interface. The amount of turbulent kinetic energy available for mixing is well-known to be directly related to wind stress and buoyancy forcing (Gordon and Corry, 1991). Wind stress typically provides the leading contribution to the turbulent kinetic energy and buoyancy the secondary contribution, with the latter dominated by the net surface heat flux. Variations in thermocline depth can therefore be related to changes in the wind stress and net surface heat flux.

During the 1997 El Niño the warmest surface waters shifted to the central Pacific and surface waters warmed to over 25 °C in the eastern Pacific. For the 1998 La Niña the warmest water is about 30 °C in the western Pacific and about 20 °C in the eastern Pacific. These changes in SST indicate the equatorial ocean absorbs heat during La Niña and transports heat westward in the subtropical ocean during El Niño (Hackert et al., 2001). This suggests that the combined effect of westerly winds and surface heat flux into the equatorial ocean could be a main driving force during ENSO events as discussed by Sun (2000). For this reason we briefly investigate here the physical relationship between air–sea fluxes and MLD during the 1997–1998 ENSO.

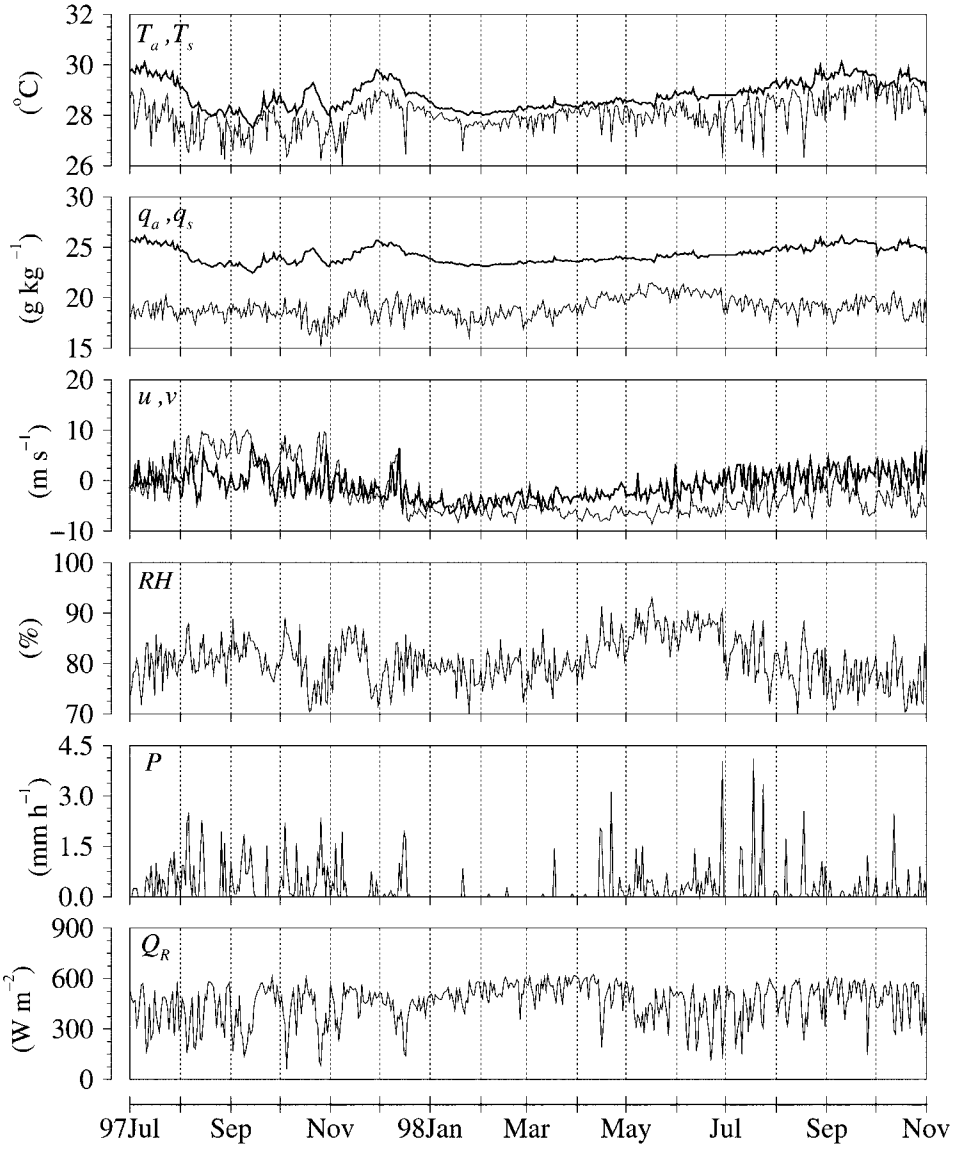

Figure 4. Time series of daily surface data from the TAO buoy at (5°N, 165°E) for July 1997 to November 1998. The observables in the panels from top to bottom are: air temperature (T_a, solid line) and sea surface temperature (T_s, thick solid line), mixing ratio at 10 m above sea level (q_a, solid line) and mixing ratio just above the sea surface (q_s, thick solid line), zonal and meridional wind speed at 10 m (u and v, solid line and thick solid line respectively), relative humidity (RH), precipitation (P), and shortwave solar radiation (Q_R).

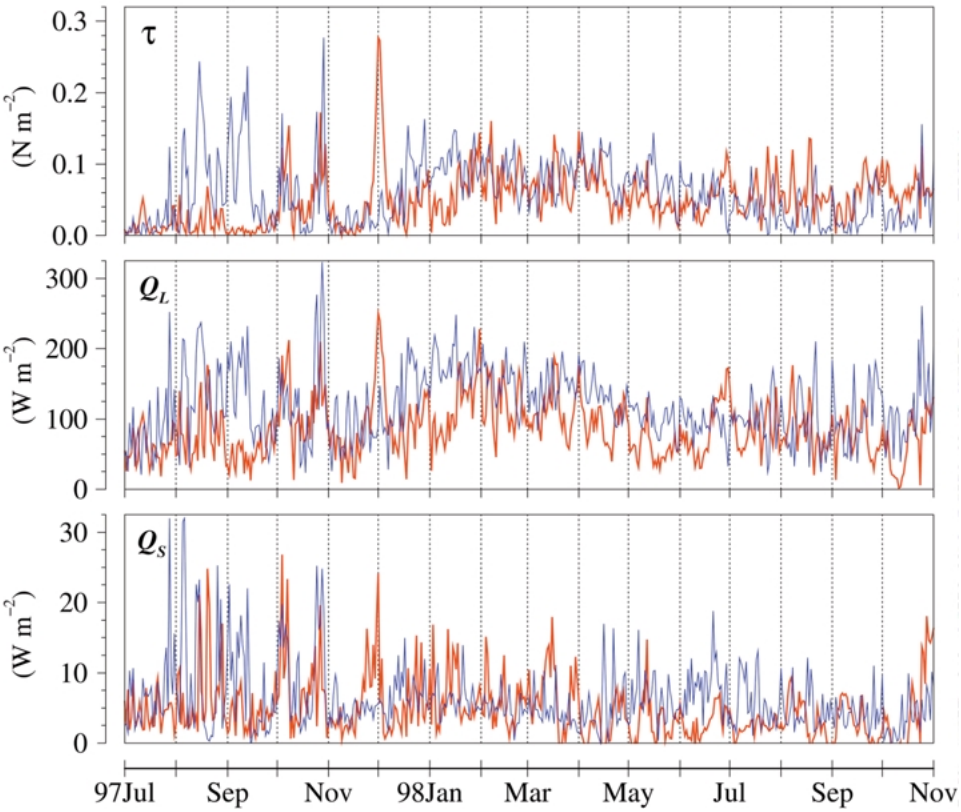

Figure 5. Time series of daily wind stress (τ), latent heat flux (Q_L) and sensible heat flux (Q_S) from 2 TAO buoys at (5° N, 165°E) and (0°Eq, 170°W). Air–sea fluxes from July 1997 through November 1998 for (5°N, 165°E) are shown with a solid blue line and those for (0°Eq, 170°W) are shown in red.

Because salinity measurements are not available for the three TAO buoys during 1997 and 1998 it is not possible to determine the MLD directly from the density variation with depth. Given that the isothermal layer depth (ILD) and MLD can be quite different in the equatorial Pacific (e.g., barrier layers (Lukas and Lindstrom, 1991; Sprintall and Tomczak, 1992; You, 1995; Kara et al., 2000b)), care must be taken to select an appropriate ILD that corresponds to the desired definition of the MLD. From a previous study (Kara et al., 2000b), it has been shown that a good approximation for an optimally defined MLD in the equatorial Ocean is an ILD determined using $\Delta T = 0.5$ °C. This ILD can be summarized in its simplest form as the depth where the temperature has changed by a fixed amount of 0.5 °C from the temperature at a reference depth of 10 m. Further details on how we determined this relationship between ILD and MLD can also be found in Kara et al. (2000c).

To examine the relationship with MLD we perform a linear correlation analysis between the daily MLD and daily averaged values of τ, Q_L and Q_S, separately. The

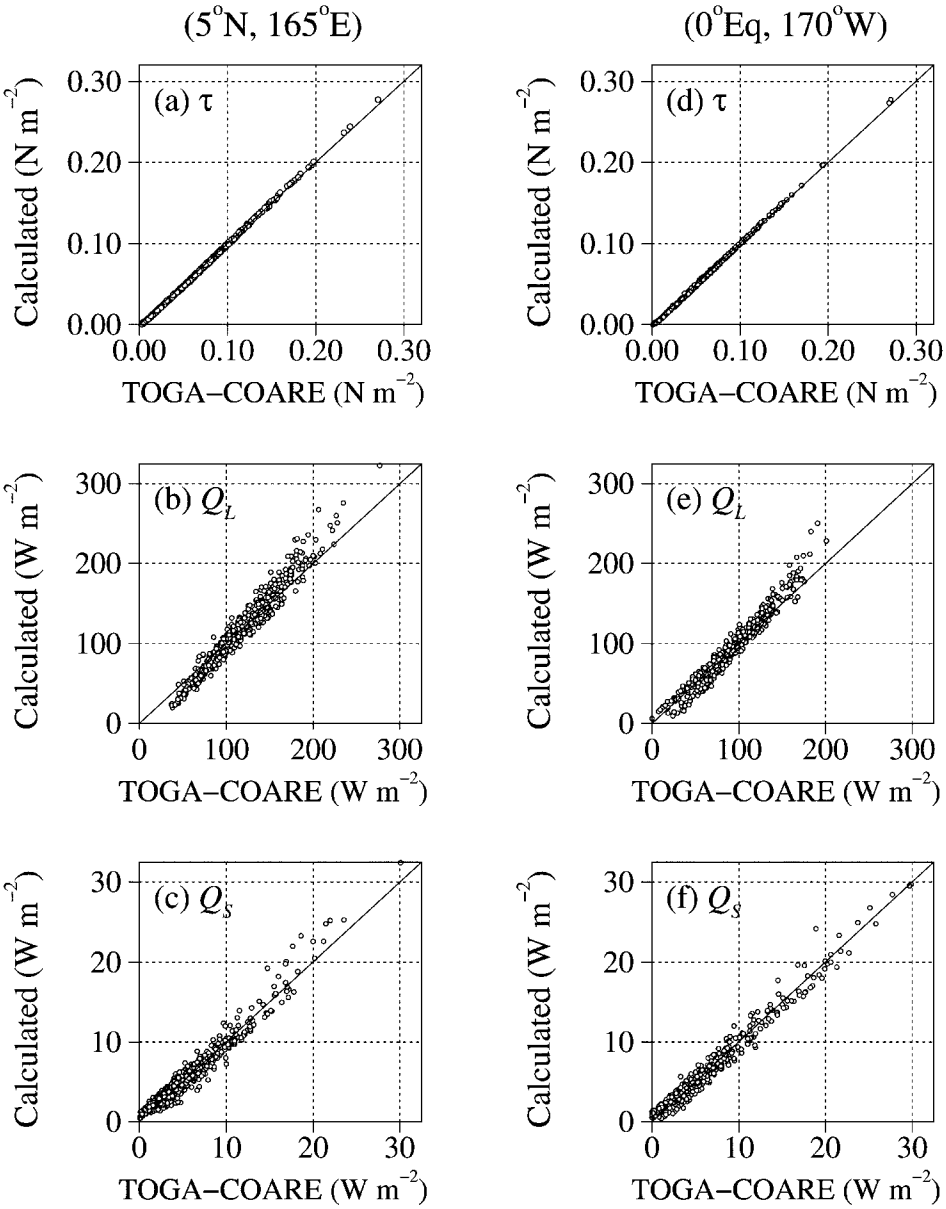

Figure 6. Scatter plots of τ, Q_L and Q_S obtained from the TOGA COARE algorithm versus our formulae during the 1997–1998 ENSO event. Air–sea fluxes from July 1997 through November 1998 at (5°N, 165°E) are shown in panels (a), (b), and (c), while those for (0°Eq, 170°W) are shown in panels (d), (e), and (f). At (5°N, 165°E) the skill scores are 0.99, 0.90, and 0.96 for τ, Q_L, and Q_S, respectively. Similarly, at (0°Eq, 170°W) there are large skill score values of 0.99, 0.89, and 0.97 for τ, Q_L, and Q_S respectively.

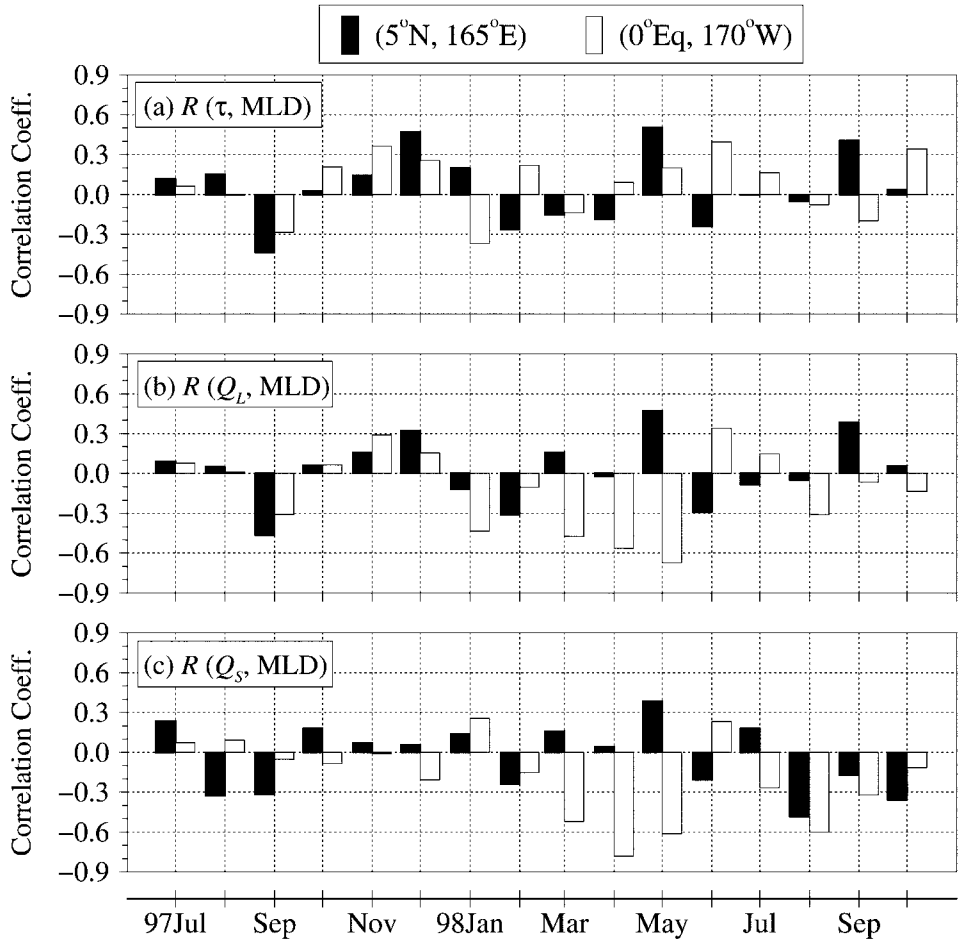

Figure 7. Correlation coefficients (R) between MLD and air–sea fluxes by month during the period July 1997 to November 1998. All R values are calculated using the total number of days for the given month.

absence of buoy data for cloudiness prevents us from determining the longwave radiative fluxes and hence examining the relationship between net surface heat flux and MLD. We consider the individual air–sea flux components to gain insight into the possible relationship with MLD. The correlation analysis is performed month by month starting from July 1997 to November 1998 (Figure 7). Moderately large values of $|R| \geq 0.4$ occur during the El Niño (August and November 1997, January–April 1998) and early La Niña (May–August 1998). The strongest correlations are noted to occur near the onset of La Niña (April–May 1998). In particular, we note that reverse correlations occur in the warm pool and in the central Pacific at this time. For example, in April 1998 the MLD is positively correlated to τ, Q_L and Q_S at (5°N, 165°E), and negatively correlated to Q_L and Q_S at (0°Eq, 170°W).

To determine whether these correlations are good or poor we apply two statistical tests. We first use the classical t-test (Chu et al., 1998) to check the null hypothesis that the MLD and air–sea fluxes are not correlated. For our monthly samples of $N = 30$ daily values, the bivariate normal distribution of

$$t_{n-2} = \frac{r\sqrt{n-2}}{\sqrt{1-R^2}}, \tag{14}$$

must lie outside the range $-0.35 \leq t_{n-2} \leq 0.35$ for R to be statistically different from zero ($R = 0$) at the 95% ($\alpha = 0.05$) confidence level based on a null hypothesis. Applying the t-test to the R values in Figure 7 we find correlations exist for the pairs of quantities (MLD, Q_L) and (MLD, Q_S) at (0°Eq, 170°W) for April–May 1998 and August 1998. Correlations also exist at (5°N, 165°E) for the quantities and months: (MLD, τ) in September and December 1997, and May 1998; (MLD, Q_L) in September 1997 and May 1998; and (MLD, Q_S) in May and August 1998.

6. Conclusions

We have introduced here simple bulk formulae for air–sea fluxes that are as accurate as those estimated by the state-of-the-art TOGA COARE algorithm in the absence of cool skin and warm layer effects. Using air–sea surface data from 96 buoys in the equatorial and North Pacific Ocean we find median RMS differences of approximately 0.003 N m^{-2}, 1 W m^{-2} and 10 W m^{-2} for the wind stress, sensible and latent heat fluxes, respectively. The accuracy of our formulae is further supported by the very high correlations (median value of $R > 0.98$) and nondimensional skill scores (median value of SS > 0.90) for the air–sea fluxes. Although our formulae were derived for open ocean conditions we found them to be as accurate with respect to the TOGA COARE estimates for NODC buoys located within U.S. coastal waters. We also evaluated the performance of our bulk formulae by examining the daily variability of wind stress, sensible and latent heat fluxes at two buoy locations in the equatorial Pacific during the 1997–1998 ENSO event. We found our formulae reproduce air–sea fluxes on daily time scales very well, and can be used for strong atmospheric and oceanic conditions that occur during such events.

The ready access to air–sea fluxes and subsurface temperatures at two TAO buoys in the equatorial Pacific motivated us to examine a possible relationship between MLD and air–sea fluxes during the 1997–1998 ENSO event. We found there is almost no relationship between MLD and the air–sea fluxes during the 1997–1998 ENSO. There is some evidence to suggest that the start of a La Niña may be identified by the correlations between MLD and air–sea fluxes. In particular, the start of the La Niña might be identified by searching for a negative

correlation between the MLD and air–sea fluxes in the eastern equatorial Pacific that occurs within a month of a positive MLD and air–sea flux correlation in the western Pacific warm pool.

Finally, we conclude our simple bulk formulae are applicable for not only open ocean conditions but also coastal regions where air–sea temperature difference plays an important role. Extending our formulae for a dependence on wave height merits future investigation. From our experience with the Naval Research Laboratory Layered Global Ocean Model, we find the greater computational efficiency of these formulae to merit the minor loss in accuracy of the estimated air–sea fluxes. We hope they will prove of value for other atmosphere and ocean GCMs.

Acknowledgements

Appreciation is extended to the director of the TAO Project Office, M. J. McPhaden, for making the meteorological data from the TAO array buoys available. Additional thanks go to P. Freitag of the TAO Project Office for his help in obtaining the meteorological data. Special thanks also go to D. Knoll of NODC for the mooring data. The latter were collected and provided by the National Data Buoy Center. Thanks is extended to J. J. O'Brien, director of the Center for Ocean-Atmospheric Prediction Studies (COAPS), the Florida State University, for his discussions regarding the 1997–1998 ENSO event. The comments of reviewers are also gratefully appreciated. This work was funded by the Office of Naval Research (ONR), and is a contribution to the Basin-Scale Prediction System project under program element 602435N and to the Dynamics of Coupled Air-Ocean Models Study under program element 61153N. This is NRL contribution number JA/7330-01-0066 and has been approved for public release.

References

Blake, R. A.: 1991, 'The Dependence of Wind Stress on Wave Height and Wind Speed', *J. Geophys. Res.* **96**, 20,531–20,545.

Buck, A. L.: 1981, 'New Equations for Computing Vapor Pressure and Enhancement Factor', *J. Appl. Meteorol.* **20**, 1527–1532.

Bunker, A. F.: 1976, 'Computations of Surface Energy Flux and Annual Air–Sea Interaction Cycles of the North Atlantic Ocean', *Mon. Wea. Rev.* **104**, 1122–1140.

Caldwell, D. R. and Elliott, W. P.: 1971, 'Surface Stresses Produced by Rainfall', *J. Phys. Oceanog.* **1**, 145–148.

Cassou, C. and Perigaud, C.: 2000, 'ENSO Simulated by Intermediate Coupled Models and Evaluated with Observations over 1970–1998. Part II: Role of the Off-Equatorial Ocean and Meridional Winds', *J. Climate* **13**, 1635–1663.

Chu, P. C., Chen, Y., and Lu, S.: 1998, 'On Haney-Type Surface Thermal Boundary Conditions for Ocean Circulation Models', *J. Phys. Oceanog.* **28**, 890–901.

Dunckel, M., Hasse, L., Krugermeyer, L., Schreiver, D., and Wucknitz, J.: 1974, 'Turbulent Fluxes of Momentum, Heat and Water Vapor in the Atmospheric Surface Layer at Sea during ATEX', *Boundary-Layer Meteorol.* **6**, 81–106.

Elsner, J. B. and Kara, A. B.: 1999, *Hurricanes of the North Atlantic: Climate and Society*, Oxford University Press, New York, 496 pp.

Fairall, C. W., Bradley, E. F., Rogers, D. P., Edson, J. B., and Young, G. S.: 1996, Bulk Parameterization of Air–Sea Fluxes for Tropical Ocean-Global Atmosphere Coupled-Ocean Atmosphere Response Experiment', *J. Geophys. Res.* **101**, 3747–3764.

Godfrey, J. S. and Beljaars, A. C. M.: 1991, 'On the Turbulent Fluxes of Buoyancy, Heat, and Moisture at the Air–Sea Interface at Low Wind Speeds', *J. Geophys. Res.* **96**, 22,043–22,048.

Gordon, C. and Corry, R. A.: 1991, 'A Model Simulation of the Seasonal Cycle in the Tropical Pacific Ocean Using Climatological and Modeled Surface Forcing', *J. Geophys. Res.* **96**, 847–864.

Gosnell, R., Fairall, C. W., and Webster, P. J.: 1995, 'The Sensible Heat of Rainfall in the Tropical Ocean', *J. Geophys. Res.* **100**, 18,437–18,442.

Hackert, E. C., Busalacchi, A. J., and Murtugudde, R.: 2001, 'A Wind Comparison Study Using an Ocean General Circulation Model for the 1997–1998 El Niño', *J. Geophys. Res.* **106**, 2345–2362.

Hurlburt, H. E., Kindle, J. C., and O'Brien, J. J.: 1976, 'Numerical-Simulation of Onset of El Niño', *J. Phys. Oceanog.* **6**, 621–631.

Isemer, H.-J., Willebrand, J., and Hasse, L.: 1989, 'Fine Adjustment of Large-Scale Air Sea Energy Flux Parameterizations by Direct Estimates of Ocean Heat Transport', *J. Climate* **2**, 1173–1184.

Kara, A. B., Rochford, P. A., and Hurlburt, H. E.: 2000a, 'Efficient and Accurate Bulk Parameterizations of Air–Sea Fluxes for Use in General Circulation Models', *J. Atmos. Oceanic Tech.* **17**, 1421–1438.

Kara, A. B., Rochford, P. A., and Hurlburt, H. E.: 2000b, 'Mixed Layer Depth Variability and Barrier Layer Formation over the North Pacific Ocean', *J. Geophys. Res.* **105**, 16,783–16,801.

Kara, A. B., Rochford, P. A., and Hurlburt, H. E.: 2000c, 'An Optimal Definition for Ocean Mixed Layer Depth', *J. Geophys. Res.* **105**, 16,803–16,821.

Lee, H.-K., Chu, P.-S., Sui, C.-H., and Lau, K.-M.: 1998, 'On the Annual Cycle of Latent Heat Fluxes over the Equatorial Pacific Using TAO Buoy Observations', *J. Meteorol. Soc. Japan* **76**, 909–923.

Lukas, R. and Lindstrom, E.: 1991, 'The Mixed Layer of the Western Equatorial Pacific Ocean', *J. Geophys. Res.* **96**, 3343–3357.

McPhaden, M. J.: 1995, 'The Tropical Atmosphere Ocean (TAO) Array is Completed', *Bull. Amer. Meteorol. Soc.* **76**, 739–741.

McPhaden, M. J.: 1999, 'Genesis and Evolution of the 1997–1998 El Niño', *Science* **283**, 950–954.

Meinen, C. S. and McPhaden, M. J.: 2000, 'Observations of Warm Water Volume Changes in the Equatorial Pacific and their Relationship to El Niño and La Niña', *J. Climate* **13**, 3551–3559.

Murphy, A. H.: 1988, 'Skill Scores Based on the Mean Square Error and their Relationships to the Correlation Coefficient', *Mon. Wea. Rev.* **116**, 2417–2424.

O'Brien, E. W. and Horsfall, F.: 1995, 'Sensitivity of the Heat Budget in a Midlatitude Ocean Model to Variations in Atmospheric Forcing', *J. Geophys. Res.* **100**, 24,761–24,772.

Perigaud, C., Melin, F., and Cassou, C.: 2000, 'ENSO Simulated by Intermediate Coupled Models and Evaluated with Observations over 1970–1998. Part I: Role of the Off-Equatorial Variability', *J. Climate* **13**, 1605–1634.

Smith, S. D.: 1989, 'Water Vapor Flux at the Sea Surface', *Boundary-Layer Meteorol.* **47**, 277–293.

Smith, S. D., Fairall, C. W., Geernaert, G. L., and Hasse, L.: 1996, 'Air–Sea Fluxes: 25 Years of Progress', *Boundary-Layer Meteorol.* **78**, 247–290.

Smith, S. R., Legler, D. M., Remigio, M. J., and O'Brien, J. J.: 1999, 'Comparison of 1997–1998 U.S. Temperature and Precipitation Anomalies to Historical ENSO Warm Phases', *J. Climate* **12**, 3507–3515.

Sprintall, J. and Tomczak, M.: 1992, 'Evidence of the Barrier Layer in the Surface Layer of Tropics', *J. Geophys. Res.* **97**, 7305–7316.

Sun, D.-Z.: 2000, 'The Heat Sources and Sinks of the 1986–1987 El Niño', *J. Climate* **13**, 3533–3550.

Wang, C. and Weisberg, R. H.: 2000, 'The 1997–1998 El Niño Evolution Relative to Previous El Niño Events', *J. Climate* **13**, 488–501.

Weisberg, R. H. and Wang, C.: 1997, 'Slow Variability in the Equatorial West-Central Pacific in Relation to ENSO', *J. Climate* **10**, 1998–2017.

Weller, R. A., Baumgartner, M. F., Josey, S. A., Fischer, A. S., and Kindle, J. C.: 1998, 'Atmospheric Forcing in the Arabian Sea during 1994–1995: Observations and Comparisons with Climatology Models', *Deep Sea Res.* **45**, 1961–1999.

White, W. B. and Cayan, D. R.: 2000, 'A Global El Niño-Southern Oscillation Wave in Surface Temperature and Pressure and its Interdecadal Modulation from 1900 to 1997', *J. Geophys. Res.* **105**, 11,223–11,242.

White, W. B. and McCreary, J. P.: 1974, 'Eastern Intensification of Ocean Spin-Down – Application to El-Niño', *J. Phys. Oceanog.* **4**, 295–303.

You, Y.: 1995, 'Salinity Variability and its Role in the Barrier Layer Formation during TOGA COARE', *J. Phys. Oceanog.* **25**, 2778–2807.

Yukimoto, S., Endoh, M., Kitamura, Y., Kitoh, A., Motoi, T., Noda, A., and Tokioka, T.: 1996, 'Interannual and Interdecadal Variabilities in the Pacific in an MRI Coupled GCM', *Clim. Dyn.* **12**, 667–683.

Zeng, X., Zhao, M., and Dickinson, R. E.: 1998, 'Intercomparison of Bulk Aerodynamic Algorithms for the Computations of Sea Surface Fluxes Using TOGA COARE and TAO Estimates', *J. Climate* **11**, 2628–2644.

Zhang, R. H. and Busalacchi, A. J.: 1999, 'A Possible Link between Off-Equatorial Warm Anomalies Propagating along the NEDD Path and the Onset of the 1997–1998 El Niño', *Geophys. Res. Lett.* **26**, 2873–2876.